Wafer-Scale Field-Effect Transistor-Type Sensor Using a Carbon Nanotube Film as a Channel for Ppb-Level Hydrogen Sulfide Detection

Shixiang Zhan, Huamei Zuo, Bin Liu, Wangping Xu, Juexian Cao, Yong Zhang,* and Xiaolin Wei*

Cite This: https://doi.org/10.1021/acssensors.3c00653

Read Online

ACCESS | Metrics & More | Article Recommendations | SI Supporting Information

ABSTRACT: Sulfur hexafluoride is widely used in power equipment because of its excellent insulation and arc extinguishing properties. However, severe damage to power equipment may be caused and a large-scale collapse of the power grid may occur when SF_6 is decomposed into H_2S, SOF_2, and SO_2F_2. It is difficult to detect the SF_6 concentration as it is a kind of inert gas. Generally, the trace gas decomposed in the early stage of SF_6 is detected to achieve the function of early warning. Consequently, it is of great significance to realize the real-time detection of trace gases decomposed from SF_6 for the early fault diagnosis of power equipment. In this work, a wafer-scale gate-sensing carbon-based FET gas sensor is fabricated on a four-inch carbon wafer for the detection of H_2S, a decomposition product of SF_6. The carbon nanotubes with semiconductor properties and the noble metal Pt are respectively used as a channel and a sensing gate of the FET-type gas sensor, and the channel transmission layer and the sensing gate layer each play an independent role and do not interfere with each other by introducing the gate dielectric layer Y_2O_3, giving full play to their respective advantages to forming an integrated sensor of gas detection and signal amplification. The detection limit of the as-prepared gate-sensing carbon-based FET gas sensor can reach 20 ppb, and its response deviation is not more than 3% for the different batches of gas sensors. This work provides a potentially useful solution for the industrial production of miniaturized and integrated gas sensors.

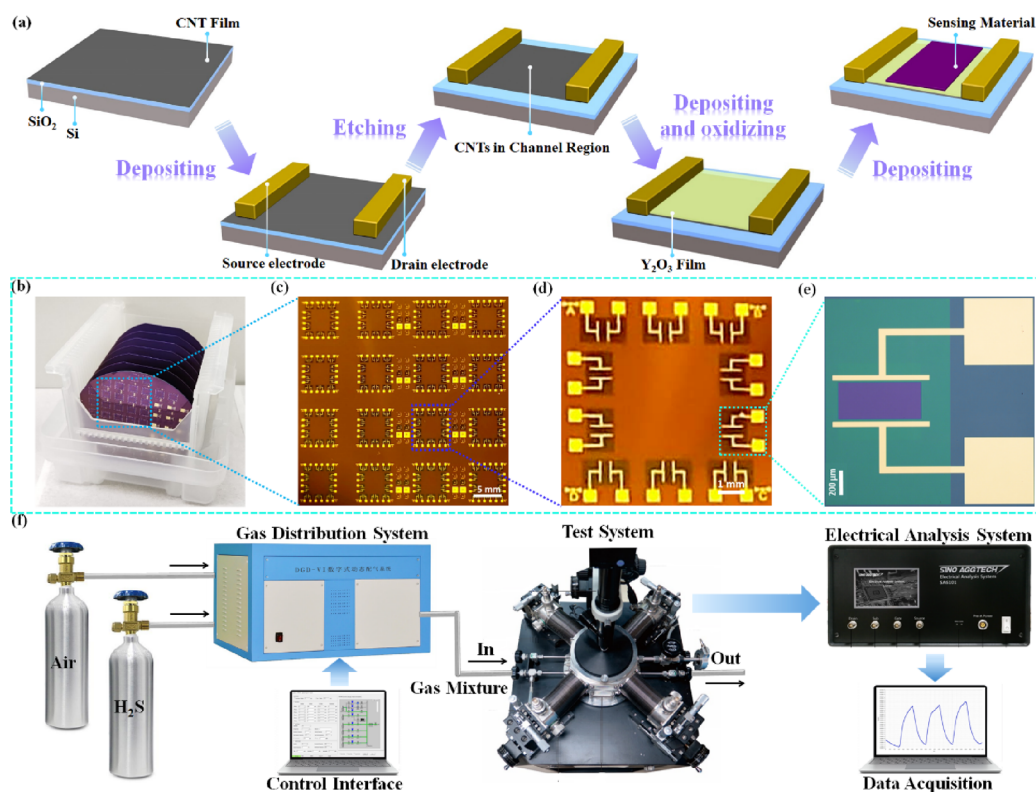**KEYWORDS:** carbon-based FET, FET gas sensor, sensing gate, trace gas detection, hydrogen sulfide
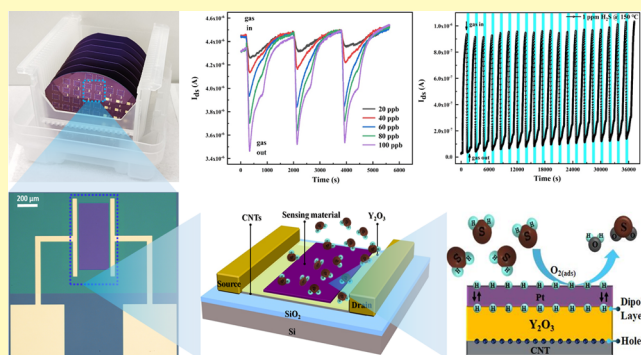
Sulfur hexafluoride (SF_6) is widely used as the insulating medium of gas insulated switchgear (GIS) because of its excellent insulation and arc extinguishing performance.[1] However, partial discharge and other factors caused by GIS insulation defects will decompose SF_6,[2] and the internal insulation performance of GIS will be degraded with the decomposition of SF_6[3] resulting in damage to power equipment and large-scale collapse of the power grid.[4] SF_6 is an inert gas and difficult to detect.[5] The usual detection method is to detect the decomposition products of SF_6, such as trace H_2S, SOF_2, and SO_2F_2, in order to achieve the function of early fault warning.[6] Therefore, it is of great significance to realize the real-time detection of trace decomposition products of SF_6 for the early fault diagnosis of GIS. At present, the technologies such as infrared absorption spectroscopy[7] and gas chromatography mass spectrometry[8] have been used to detect SF_6 decomposed gas. Nevertheless, these methods have a long detection cycle, high cost, and large volume and are inconvenient to use. Therefore, how to conveniently conduct rapid and real-time analysis of decomposed gas has become an urgent problem to be solved. In contrast, the resistive gas sensor[9] is expected to be used for the detection of SF_6

decomposition gas because of its simple operation,[10] miniaturization,[11] low cost, and real-time monitoring.[12] However, it is difficult for the resistive gas sensor to meet the actual detection requirements of trace decomposition gas because the electrical signal generated by trace gas is too weak to be detected, and it is easy to be interfered by other gases. Accordingly, it remains challenging to achieve accurate detection of trace SF_6 decomposition products with simple operation, real-time monitoring, and low cost.

In recent years, with the rapid development of semiconductor technology and micro−nano processing technology, a field-effect transistor (FET) gas sensor[13] has attracted wide attention because of its high sensitivity,[14] miniaturization,[15] and ease of integration. The weak signal caused by trace gas is

A

Figure 1. (a) Schematic representation of the fabrication procedure of the gate-sensing carbon-based FET gas sensor. (b) Photograph image of the wafer-scale gate-sensing carbon-based FET gas sensor fabricated on a four-inch wafer. (c) Optical micrograph of a total of 16 gas sensor arrays arranged in 4 × 4. (d) Further magnified optical micrograph of a sensor array with 10 gas sensors. (e) Optical micrograph of a gate-sensing carbon-based FET gas sensor. (f) Schematic diagram of the gas sensing measurement platform.

easily detected by an FET gas sensor because of the amplification effect of FET,[16] which is expected to detect trace SF_6 decomposition products. At present, the channel materials used in the FET mainly include single-crystal Si and its derivatives,[17] carbon nanotubes,[18] graphene,[19] transition metal dichalcogenides,[20] and so on. Among them, carbon nanotubes (CNTs) are considered to be one of the most potential nanomaterials as transistor channels due to their outstanding advantages such as ultrasmall size, high mobility, and extremely stable chemical properties.[21] The experimental data show that the carrier mobility of a typical silicon field-effect transistor is 10^3 cm^2/(V·s) at room temperature, and that of CNTs is up to 10^5 cm^2/(V·s),[22] which is about 100 times that of silicon. As a consequence, under the same channel length, the higher the carrier mobility is, the larger the transconductance, the larger the on-state current, and the faster the speed of the device can be achieved.[23] In addition, Peng et al. proposed undoped fabrication technology of CNT CMOS devices,[24] which effectively avoids the injection of impurities in silicon-based FETs, making the process much simpler. Zhang et al. used undoped technology to evaporate Pd nanoparticles on the surface of CNT films to form FET gas sensors with a back gate structure, in which the detection limit of hydrogen can reach 89 ppb.[25] When the CNTs are directly exposed to the target environment as a channel, it will form an interaction mechanism with the sensing material to the target gas, and other gases in the air will also affect the channel conduction, resulting in the complexity of the channel conduction and the lack of stability of the sensor.

In this work, a gate-sensing carbon-based FET gas sensor is designed and fabricated on a four-inch wafer covered with a random network of semiconducting CNT films. The sensor takes a Pt film as a sensing gate without external leads. The introduction of Y_2O_3 as the gate dielectric layer makes the CNT network film just as a channel, which aims to overcome the influence caused by channel exposure. In this way, the channel transmission layer and the sensing gate layer can give full play to their respective advantages. It is expected that this work can achieve accurate real-time detection of trace H_2S in SF_6 decomposition products for early fault warning of GIS and provide a strategy for the development and application of miniaturized and integrated gas sensor chips.

■ EXPERIMENTAL DETAILS

The carbon-based wafer used in this work was obtained by depositing randomly arranged CNTs on the surface of a four-inch Si/SiO$_2$ wafer by immersion, and the detailed process can be referred in the work of Zhang's research team.[25] The gate-sensing carbon-based FET gas sensor was fabricated on a four-inch carbon-based wafer using the following lithography-based micro−nano process technology, as shown in Figure 1a. First, the source electrode (S) and the drain electrode (D) regions were defined on a four-inch carbon-based wafer by UV lithography (EVG-610), and Ti/Pd/Au (0.3 nm/20 nm/40 nm) was deposited as a contact electrode by electron beam evaporation (DE400DHL) at the deposition rates of 0.1, 1, and 1 Å/s, respectively. After that, a photolithography machine was used to expose the part except the channel, and a reactive ion etching machine (Haasrode-R200a) was used to introduce oxygen for 60 s to react with the CNTs to etch off the excess CNTs to form a channel with a length of 300 μm and a width of 600 μm. Third, an yttrium (Y) film of 3 nm was evaporated on the channel at a rate of 0.1 Å/s by electron beam evaporation, and an yttrium oxide (Y_2O_3) film of about 5 nm was formed by thermal oxidation at 270 °C for 30 min. Then, the third step was repeated one more time, and a layer of Y_2O_3 with about
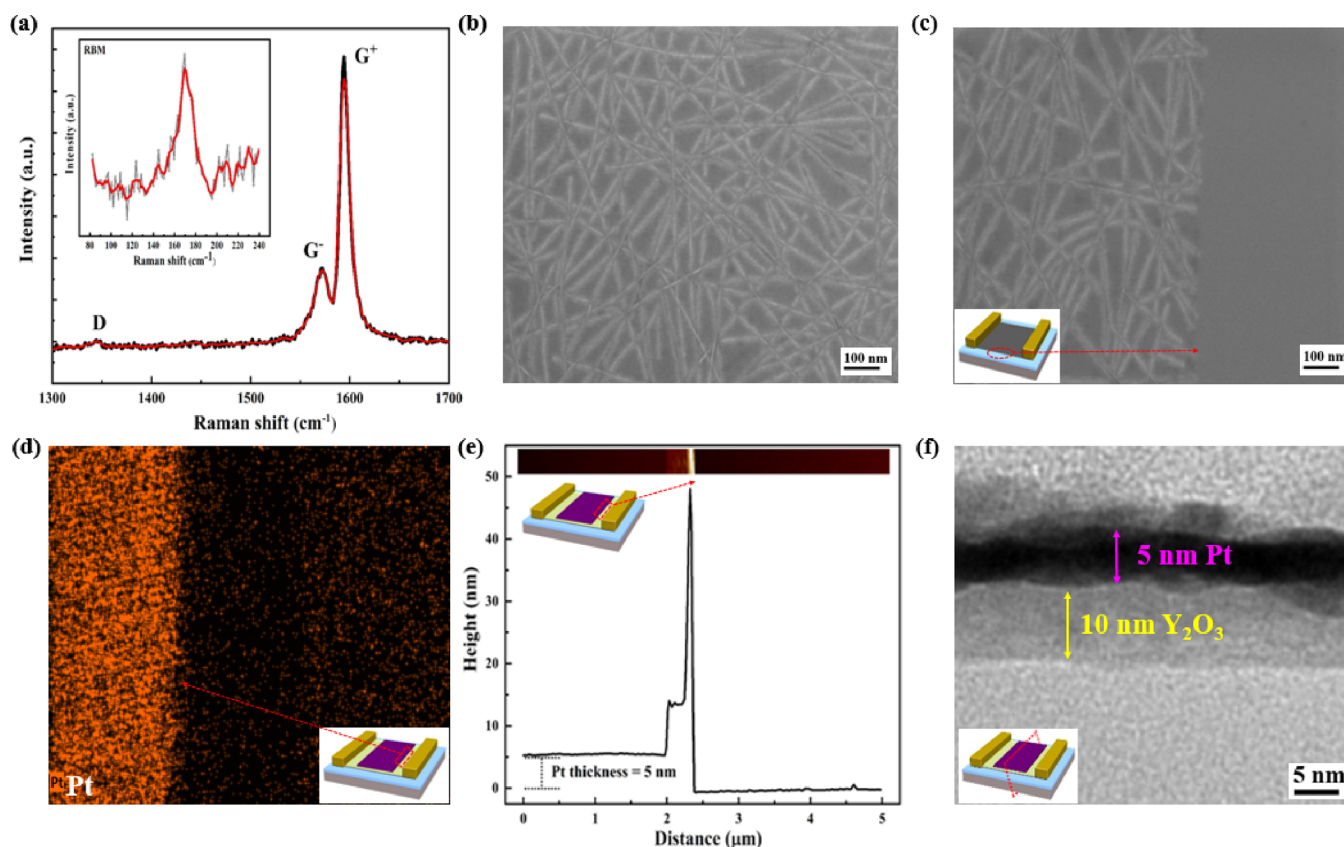
Figure 2. (a) Raman spectrum of the CNT film. FESEM images of (b) CNT film and (c) CNTs after etching. (d) EDS mapping and (e) AFM characterization of the sensing gate layer. (f) HRTEM image of the cross section of the gate-sensing carbon-based FET gas sensor.

10 nm was formed as the gate dielectric layer of the FET. Finally, a Pt film of 5 nm was sputtered on the gate dielectric layer as a sensing gate layer at a rate of 0.33 nm/s by magnetron sputtering (DE500). The as-fabricated wafer-scale gate-sensing carbon-based FET gas sensor in a four-inch wafer is shown in Figure 1b, in which Figure 1c shows a total of 16 sensor arrays arranged in 4×4, and each sensor array contains 10 sensors as shown in Figure 1d. The optical micrograph of a gate-sensing carbon-based FET gas sensor is shown in Figure 1e.

The properties of CNT channels were evaluated by Raman spectroscopy (inVia) and field-emission scanning electron microscopy (FESEM, Sigma 500). Energy-dispersive spectroscopy (EDS, XFlash 6) and atomic force microscopy (AFM, Dimension XR) were used to characterize the composition, surface roughness, and thickness of the sensing gate. The structure of the sensor was also observed by high-resolution transmission electron microscopy (HRTEM, JEM-2100). The electrical properties of the carbon-based FETs were tested using a semiconductor characterization analyzer (Keithley 4200A-SCS) and a probe station (ESP150RF). In order to improve the stability, the sensors were aged for 10 h before the gas sensitivity test. The gas sensing performances of the sensor were measured by the gas sensing measurement platform composed of the gas distribution system (DGD-VI), the test system (AES-4TH), and electrical analysis system (SA6101), and the schematic diagram of the gas sensing measurement platform is shown in Figure 1f. The dry compressed air (79% N_2 and 21% O_2) and standard H_2S gas (100 ppm) used in this work were purchased from Dalian Special Gases Co., Ltd. and calibrated by a Fourier transform infrared spectrometer (Spectrum 100). The mass flow controllers in the gas distribution system were adopted to control the gas flow and humidity, and the standard H_2S gas was diluted into dry compressed air to obtain the target gases with different concentrations. The preparation process of the interfering gases (e.g., CO, SF_6, SO_2, etc.) was similar to that of the target gas. During the whole test, we used the same response and recovery time for the

gas detection of different concentrations, which improves the simplicity in practical application.[26] Moreover, the time of introducing air and target gas in turn was 20 and 10 min, respectively. In this work, the sensor response value is defined as

$$\text{response} = \frac{|I_g - I_a|}{I_a} \times 100\ (\%),$$

where I_g and I_a represent the maximum value of the current change when the gas sensor is exposed to the target gas and air, respectively.[27]

RESULTS AND DISCUSSION

In order to evaluate the quality of the CNT film, the Raman spectrum of the CNT film (the excitation wavelength of the laser is 532 nm) is characterized as shown in Figure 2a. The characteristic G^+ and G^- peaks of CNTs near 1590 and 1570 cm^{-1} can be seen, respectively, which come from the stretching vibration of carbon−carbon bonds along the axial and circumferential directions of CNTs, severally. It can be observed that the peak shape of the G^- peak is a symmetrical Lorentzian peak, indicating that CNTs are of semiconductor property,[28] which is the prerequisite for constructing an FET with CNTs as a channel. In addition, the D peak near 1350 cm^{-1} is a secondary scattering peak related to the defects, and the ratio of the G^+ peak to the D peak reflects the degree of defects of CNTs.[29] The high ratio of I_{G+}/I_D indicates that there are few defects in CNTs, greatly reducing the elastic scattering process caused by defects, which ensures the good electrical performance of the carbon-based FET. As can be seen from the inset of Figure 2a, a narrow radial breathing mode (RBM) peak appears at 170 cm^{-1}, and the diameter distribution of about 1.5 nm for the CNTs is obtained according to the formula $\omega = 248/d$ (nm), where ω and d are the RBM Raman shift and
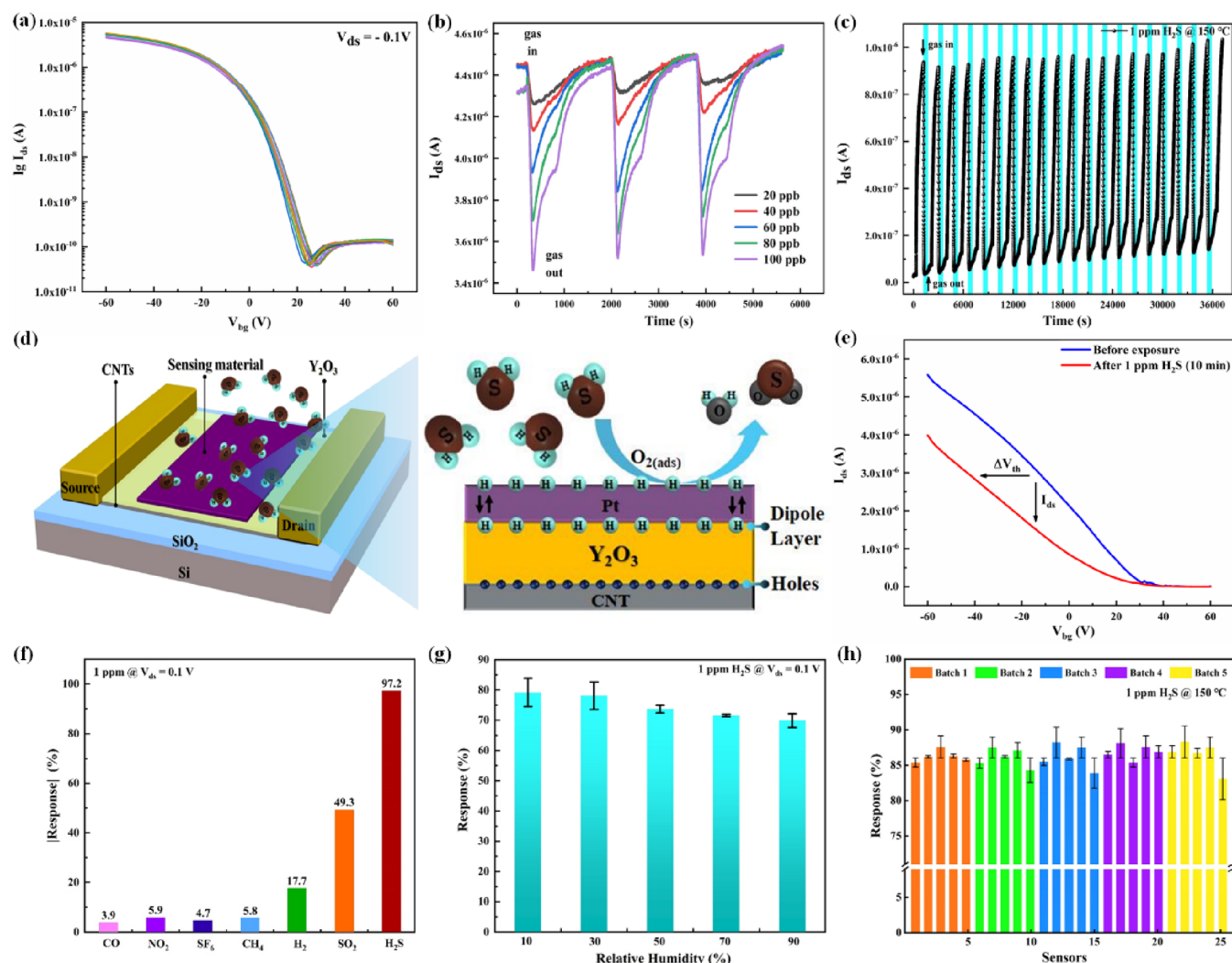
Figure 3. (a) Transfer characteristic curves of 30 carbon-based FETs. Transient response/recovery curves of the gate-sensing carbon-based FET gas sensor (b) in the concentration range of 20−100 ppb H_2S and (c) 20 repeated tests at 1 ppm H_2S. (d) Schematic representation of the sensing mechanism of the gate-sensing carbon-based FET gas sensor. (e) Transfer characteristic curve of the gate-sensing carbon-based FET gas sensor before and after the introduction of H_2S. Response values of the gas sensor toward (f) 1 ppm of different gases and (g) 1 ppm H_2S with different relative humidities. (h) Response values to 1 ppm H_2S for a total of 25 gas sensors randomly selected from different fabrication batches.

diameter of the CNTs, respectively.[30] In order to characterize the morphology and distribution, the FESEM image of the CNT film is shown in Figure 2b. It can be seen that the randomly arranged CNTs are uniformly and densely covered on the Si/SiO$_2$ surface to form CNT films. The uniform and nonoriented morphology of CNT films allows us to fabricate devices at random positions on the carbon-based wafer without positioning the fabrication area, which greatly simplifies the batch fabrication process of wafer-scale carbon-based FET gas sensors, beneficial for increasing the utilization of CNTs and reducing the processing cost. In addition, the thickness of the CNT film is characterized by AFM, as shown in Figure S1. It can be seen that CNTs are randomly stacked on the wafer to form a CNT film with a thickness of about 5 nm. The thickness of the CNT film is at the nanometer level, which can prevent the CNT stack from being too thick to cause the shielding effect between the CNTs to be prominent. In order to prevent the leakage and electrical crosstalk between devices, the redundant CNTs outside the channel should be etched by reactive ion etching, and the FESEM image of the boundary region of the CNT channel is given to verify the etching effect

as shown in Figure 2c. It can be seen that the CNTs in the channel region on the left side are not affected after etching, while the CNTs on the right side are etched very cleanly by reacting with oxygen without any CNTs remaining, which indicates that the etching process successfully forms a channel region with controllability and accuracy. Further, the sensing gate fabricated by photolithography combined with the sputtering process is characterized by EDS, and its EDS-mapping is depicted in Figure 2d. It can be found that there is a very small amount of Pt in the region outside the sensing gate, which is caused by the inevitable background noise in the EDS characterization process. It can be seen from the figure that the intensity of the characteristic X-ray of Pt on the left side is much larger than that of the background noise, which proves the existence of a large number of Pt elements. The surface morphology of the sensing gate is further analyzed by AFM, and the characterization result is shown in Figure 2e. The thickness of the sensing gate is about 5 nm, and the surface roughness is about 0.2 nm, indicating that the sensing gate composed of the Pt element is of a uniform and flat surface. It should be noted that the sharp peak near 2.5 μm in

the figure represents the thickness of the remaining photoresist after the stripping process, which is used to protect the sensing gate from the leakage of S/D electrodes. In order to verify the structure of the gate-sensing carbon-based FET gas sensor, the HRTEM image of the cross section of the sensor is observed as shown in Figure 2f, and the inset in the figure shows the position of the cross section where the sensor is cut. A sensing-gate layer with a thickness of about 5 nm can be observed (also as shown in AFM), and a dielectric layer with a thickness of about 10 nm is found under the sensing gate. From Figure S2, the lattice fringes with the interplanar distances of 0.227 and 0.433 nm are observed in the sensing gate layer and the dielectric layer, corresponding to the (111) plane of Pt[31] and the (211) plane of Y_2O_3[32] respectively.

A carbon-based FET gas sensor is designed and formed based on the FET with CNTs as a channel, and the electrical performance of the carbon-based FET plays a decisive role in the gas sensing performance of the sensor. The good consistency of carbon-based FETs is the premise of the gate-sensing carbon-based FET gas sensor with gas sensing response consistency. The transfer characteristic curves of 30 FETs randomly selected from different areas of the whole four-inch carbon-based wafer are shown in Figure 3a, and the circuit connection is shown in Figure S3. Note that the gas sensing material is used as a sensing gate without external leads for the proposed sensor, where a gate bias cannot be applied. Hence, the electrical performance is tested by applying different back gate voltages (V_{bg}) from the substrate of the sensor. The test is performed under the condition that V_{ds} = −0.1 V; V_{bg} increased from −60 to 60 V in steps of 1 V. It can be seen from Figure 3a that the electrical properties of the 30 FETs have good consistency. The relevant performance parameters of the FET are extracted, which exhibit a subthreshold slope swing of 5100 mV/dec, a transconductance of 0.11 μS, and a threshold voltage of −3.7 V for this carbon-based FET. The on−off ratio (I_{on}/I_{off}) of all FETs is more than 10^4, and the turn-off current is less than 1 nA. The as-prepared carbon-based FET is a typical p-channel enhancement device because the carbon-based FET uses a high work function metal Pd (5.6 eV) as the contact electrode,[33] which is above the Fermi level of the intrinsic CNTs (about 4.5 eV),[34] and the Fermi level of this metal is close to the valence band of CNTs. Therefore, it can form a barrier-free contact to holes with the valence band of CNTs[35] but form a large barrier to electrons with the conduction band of CNTs,[36] resulting in the working current mainly coming from holes. The working principle of carbon-based FETs is as follows: the CNTs form a Schottky contact with the S/D electrodes that has substantially no barrier height to holes. The appropriate gate voltage is applied through the gate to control the hole concentration in the active layer composed of CNTs, and then, the corresponding drain-source voltage is applied to obtain the drain-source current (I_{ds}) that changes with the gate voltage as shown in Figure 3a. In order to determine the optimal operating temperature of the sensor before the gas sensitivity test, the test temperature is gradually raised from 25 to 200 °C, and the response value of the sensor to 1 ppm H_2S is recorded, as shown in Figure S4. It can be seen that the maximum response value (97.3%) is obtained at 150 °C; consequently, the operating temperature of the sensor is set at 150 °C. In addition, through characterizing the thicknesses of the different gates by AFM, the influence of the gate with different thicknesses on the performance of the sensor is investigated as shown in Figures S5 and S6. It can be

seen that the thicknesses of the sensing gate layer are 1, 3, 5, 7, and 9 nm individually, which are consistent with the experimental expectation in the preparation process, and the corresponding gas sensing responses of these sensors are 43.5, 86.7, 97.3, 64.6, and 97.2%, respectively. When the thicknesses of the gate are 5 and 9 nm singly, there is a large response value (about 97%) to 1 ppm H_2S. From a cost point of view, 5 nm is chosen as the optimal thickness of the sensing gate layer. As shown in Figure 3b, in order to evaluate the detection capability of the gate-sensing carbon-based FET gas sensor for trace H_2S, the transient response/recovery curves of the I_{ds} are measured in the concentration range of 20−100 ppb. It can be seen that the gas sensor has a significant response to 20 ppb H_2S gas, which meets the requirements of applications such as meat quality assessment,[37] halitosis diagnosis,[38] and early warning of electrical equipment.[39] Moreover, it is also found that the gas sensor is still unstable after H_2S is introduced for a period of time, which is mainly due to the fact that the sensor fails to reach the dynamic equilibrium of gas adsorption and desorption during the period of time when H_2S is introduced. Figure S7 shows the linear fitting curve of the response for the sensor at 20−100 ppb H_2S, and the linear correlation coefficient is 0.99985, indicating that the response of the sensor at a 20−100 ppb H_2S concentration has a good linear increase. The transient response/recovery curve of the sensor is further tested at a higher concentration of 200 ppb−1 ppm H_2S, and the results are shown in Figure S8. It can be seen that the variation of I_{ds} increases with the increase of H_2S concentration, and the response value reaches about 97% at 1 ppm. As shown in Figure 3c, in order to verify the response/recovery ability of the carbon-based FET gas sensor, 20 repeated tests are conducted on the sensor at 1 ppm H_2S, and the sensor shows stable and reliable response/recovery behavior and the consistent response value. The variation of I_{ds} in 20 repeated response/recovery tests of the gas sensor is further measured in Figure 3c, the average variation of I_{ds} is calculated to be 0.87 μA as shown in Figure S9, and the maximum deviation is 0.02 μA (2.3%).

It is well-known that the gate of a conventional FET is used to apply a bias to regulate the current in the channel. In this work, the gas sensing material is used as a sensing gate without external leads, and the interaction between the sensing gate and the target gas can cause the change in the channel current. The detailed possible sensing mechanism is shown in Figure 3d. When the gas sensor is exposed to the target gas, the following reactions will occur on the surface of the sensing gate:

$$H_2S \rightarrow 2H_a + S_a \tag{1}$$

$$2H_a + \frac{1}{2}O_2(ads) \rightarrow H_2O \tag{2}$$

$$S_a + O_2(ads) \rightarrow SO_2 \tag{3}$$

H_2S molecules are catalytically dehydrogenated through the sensing gate to produce hydrogen atoms and sulfur atoms on the sensing gate (eq 1),[40,41] and sulfur atoms and some hydrogen atoms react with oxygen adsorbed on the surface of the sensing gate to produce H_2O and SO_2, respectively (eqs 2 and 3).[42] Some hydrogen atoms penetrate the sensing gate layer[43] and diffuse to the interface between the sensing gate layer and the gate dielectric layer to form a dipole layer.[44] Part of the carriers in the channel are fixed at the interface between

the channel and the gate dielectric layer by a dipole potential,[45] which leads to the decrease of the concentration of carriers participating in the conduction in the channel, resulting in the decrease of I_{ds} and the shift of threshold voltage of the gas sensor.[14] Moreover, it can be seen from Figure 3e that the interaction between H_2S and the sensitive gate will shift the transfer characteristic curve of the sensor. I_{ds} decreases obviously, and the threshold voltage shifts to the negative direction, which proves that the amplification effect of the FET brings high sensitivity to the sensor. In this work, Y_2O_3 is used as a gate dielectric layer because it is an ideal high-κ gate material (dielectric constant is 16), and the wettability between Y_2O_3 and CNTs is good.[46] Additionally, Y_2O_3 can be uniformly grown on the surface of the CNTs without reducing key indexes such as gate capacitance and drain current of an FET. With the introduction of the gate dielectric layer, the channel transmission layer and the sensing gate layer each play an independent role and do not interfere with each other,[45] giving full play to their respective advantages to forming an integrated sensor of gas detection and signal amplification, which is the main reason that the gas sensor can detect trace gases at the ppb level. On the other hand, the introduction of the gate dielectric layer isolates the CNT channel from the influence of gas molecules,[25] and the gas reaction process occurs only on the sensing gate layer, which ensures the continuous and stable amplification effect of the channel on a gate signal, realizing the stable and reliable response/recovery capability. To further demonstrate the effect of the Y_2O_3 gate dielectric layer on the sensor performance, Pt is directly deposited on CNTs to form a channel-exposed carbon-based FET gas sensor, which makes it similar to a chemiresistor gas sensor. For the chemiresistor gas sensor, the electronic interaction between the gas and the sensing material can cause the change in the carrier number of the sensing material, which leads to the change of the sensor current. The response of the sensor at 1 ppm H_2S is tested for 5 cycles, as shown in Figure S10. The results show that the gas sensing response of the sensor to 1 ppm H_2S is about 15.6%, which is much smaller than that of the gate-sensing carbon-based FET gas sensor. This is mainly due to the direct participation of the channel in the gas sensing response, which cannot achieve effective amplification of the electrical signal. In addition, the sensor has the phenomenon of baseline drift.

In order to verify the ability of the carbon-based FET gas sensor to identify the target gas in the application environment, further investigations are performed on the selectivity, antihumidity interference ability, and long-term stability.[47] The response of the carbon-based FET gas sensor toward 1 ppm of different gases is shown in Figure 3f. The sensor shows a better response to H_2S, which means that the gas sensor has better selectivity to H_2S. The antihumidity ability is commonly used as another important parameter to evaluate the performance of gas sensors, and Figure 3g shows the response of the carbon-based FET gas sensor to 1 ppm H_2S with different relative humidity conditions. It is observed that the response value of the gas sensor decreases slightly with the increase of humidity in the range of 10−90% relative humidity. The average response value of the same sensor is about 74.5% at different relative humidities, and the maximum response deviation of the same sensor is 4.7% at different relative humidities, which confirms that the proposed gate-sensing carbon-based FET gas sensor is of good antihumidity interference. Figure S11 shows the long-term stability of the

sensor toward 1 ppm H_2S within 40 days. The response value of the gas sensor is reduced by 10% from 97%, and it still has a high response (87%) to H_2S after 40 days, proving that the as-prepared gas sensor has the ability to work stably for a long time. On the other hand, in order to further verify the reliability and uniformity of the fabrication process for the wafer-scale carbon-based FET H_2S sensor, five carbon-based FET gas sensors are randomly selected from different fabrication batches for gas sensing measurement, and the results are shown in Figure 3h. The response deviation of the gate-sensing carbon-based FET gas sensors from the different batches is not more than 3%, and the good consistency between different batches of gas sensors makes it possible to realize the industrial production of the sensor.

■ CONCLUSIONS

In this work, the gate-sensing carbon-based FET gas sensor is proposed for the trace H_2S from the decomposition of SF_6 detection, which can achieve the wafer-scale fabrication in a four-inch wafer. A gate dielectric layer composed with Y_2O_3 is introduced in the gate-sensing carbon-based FET gas sensor, which makes the channel transmission layer and the sensing gate layer each play an independent role and do not interfere with each other, giving full play to their respective advantages to form an integrated sensor of gas detection and signal amplification. The as-prepared gas sensor can realize the detection of trace H_2S with a detection limit of 20 ppb and shows stable and reliable response/recovery behavior. The maximum deviation of the change of I_{ds} is 0.02 μA (2.3%) in 20 repeated response tests. The sensor also has good antihumidity interference and long-term stable operation, with a maximum deviation of about 4.7% in the relative humidity range of 10−90%. In addition, the fabrication process of the sensor has good compatibility with the traditional CMOS processing technology, and the wafer-scale batch fabrication of the sensors ensures the consistency of the sensing performance. The response deviation of the gate-sensing carbon-based FET gas sensors from the different batches to H_2S is not more than 3%. It is expected that this work will provide approaches for the development and application of wafer-scale sensor chips for trace gas detection.

■ ASSOCIATED CONTENT

Ⓢ Supporting Information

The Supporting Information is available free of charge at https://pubs.acs.org/doi/10.1021/acssensors.3c00653.

> AFM characterization of the thickness of the CNT film (Figure S1), HRTEM image of the sensing gate layer and the dielectric layer (Figure S2), schematic diagram of the circuit connection for the electrical performance measurement (Figure S3), response values of the gate-sensing carbon-based FET gas sensor at different operating temperatures (Figure S4), AFM character-izations of the sensing gate layer with different thicknesses (Figure S5), response values of the gate-sensing carbon-based FET gas sensor with different thicknesses of the gate (Figure S6), linear fitting curve of the response for the gate-sensing carbon-based FET gas sensor at 20−100 ppb H_2S (Figure S7), transient response/recovery curves of the gate-sensing carbon-based FET gas sensor at 200 ppb−1 ppm H_2S (Figure S8), variation of I_{ds} in 20 repeated response/recovery

tests of the gate-sensing carbon-based FET gas sensor at 1 ppm H_2S (Figure S9), transient response/recovery curves of the channel-exposed carbon-based FET gas sensor at 1 ppm H_2S (Figure S10), and response values of the gate-sensing carbon-based FET gas sensor toward 1 ppm H_2S within 40 days (Figure S11) (PDF)

■ AUTHOR INFORMATION

Corresponding Authors

Yong Zhang − *School of Physics and Optoelectronics & Hunan Institute of Advanced Sensing and Information Technology, Xiangtan University, Xiangtan, Hunan 411105, P. R. China;* ◉ orcid.org/0000-0002-0118-1849; Email: zhangyong@xtu.edu.cn

Xiaolin Wei − *School of Physics and Optoelectronics & Hunan Institute of Advanced Sensing and Information Technology, Xiangtan University, Xiangtan, Hunan 411105, P. R. China; College of Physics and Electronics Engineering, Hengyang Normal University, Hengyang 421002, P. R. China;* ◉ orcid.org/0000-0002-8548-5793; Email: xlw@xtu.edu.cn

Authors

Shixiang Zhan − *School of Physics and Optoelectronics & Hunan Institute of Advanced Sensing and Information Technology, Xiangtan University, Xiangtan, Hunan 411105, P. R. China*

Huamei Zuo − *School of Physics and Optoelectronics & Hunan Institute of Advanced Sensing and Information Technology, Xiangtan University, Xiangtan, Hunan 411105, P. R. China*

Bin Liu − *School of Physics and Optoelectronics & Hunan Institute of Advanced Sensing and Information Technology, Xiangtan University, Xiangtan, Hunan 411105, P. R. China*

Wangping Xu − *School of Physics and Optoelectronics & Hunan Institute of Advanced Sensing and Information Technology, Xiangtan University, Xiangtan, Hunan 411105, P. R. China;* ◉ orcid.org/0000-0003-0229-3049

Juexian Cao − *School of Physics and Optoelectronics & Hunan Institute of Advanced Sensing and Information Technology, Xiangtan University, Xiangtan, Hunan 411105, P. R. China*

Complete contact information is available at:
https://pubs.acs.org/10.1021/acssensors.3c00653

Notes

The authors declare no competing financial interest.

■ REFERENCES

(1) Ju, T.; Fan, L.; Xiaoxing, Z.; Qinghong, M.; Jiabin, Z. Partial discharge recognition through an analysis of SF_6 decomposition products part 1: decomposition characteristics of SF_6 under four different partial discharges. *IEEE Trans. Dielectr. Electr. Insul.* **2012**, *19*, 29−36.

(2) Zeng, F.; Tang, J.; Zhang, X.; Pan, J.; Yao, Q.; Hou, X. Influence regularity of trace H_2O on SF_6 decomposition characteristics under partial discharge of needle-plate electrode. *IEEE Trans. Dielectr. Electr. Insul.* **2015**, *22*, 287−295.

(3) Foruzan, E.; Akmal, A. A. S.; Niayesh, K.; Lin, J.; Sharma, D. D. Comparative study on various dielectric barriers and their effect on breakdown voltage. *High Volt.* **2018**, *3*, 51−59.

(4) Zhang, L.; Han, X.; Li, J. Partial Discharge Detection and analysis of needle-plane defect in SF_6 under negative oscillating lightning impulse voltage based on UHF method. *IEEE Trans. Dielectr. Electr. Insul.* **2017**, *24*, 296−303.

(5) Cui, H.; Zhang, X.; Zhang, J.; Zhang, Y. Nanomaterials-based gas sensors of SF_6 decomposed species for evaluating the operation status of high-voltage insulation devices. *High Volt.* **2019**, *4*, 242−258.

(6) Fu, Y.; Yang, A.; Wang, X.; Murphy, A. B.; Li, X.; Liu, D.; Wu, Y.; Rong, M. Theoretical study of the neutral decomposition of SF_6 in the presence of H_2O and O_2 in discharges in power equipment. *J. Phys. D: Appl. Phys.* **2016**, *49*, No. 385203.

(7) Dong, M.; Zhang, C.; Ren, M.; Albarracin, R.; Ye, R. Electrochemical and infrared absorption spectroscopy detection of SF_6 decomposition products. *Sensors* **2017**, *17*, 26−27.

(8) Cai, W.; Tang, J.; Cheng, L.; Zhang, C.; Fan, M.; Zhou, Q.; Yao, Q. Detection of SF_6 decomposition components under partial discharge by photoacoustic spectrometry and its temperature characteristic. *IEEE Trans. Instrum. Meas.* **2016**, *65*, 1343−1351.

(9) Zhang, S.; Zhang, P.; Wang, Y.; Ma, Y.; Zhong, J.; Sun, X. Facile fabrication of a well-ordered porous Cu-doped SnO_2 thin film for H_2S sensing. *ACS Appl. Mater. Interfaces* **2014**, *6*, 14975−14980.

(10) Sun, Y.; Hu, J.; Zhang, Y. Visible light assisted trace gaseous NO_2 sensor with anti-humidity ability via LSPR enhancement effect. *Sens. Actuators, B* **2022**, *367*, No. 132032.

(11) Peng, X.; Liu, J.; Tan, Y.; Mo, R.; Zhang, Y. A CuO thin film type sensor via inkjet printing technology with high reproducibility for ppb-level formaldehyde detection. *Sens. Actuators, B* **2022**, *362*, No. 131775.

(12) Vuong, N. M.; Chinh, N. D.; Huy, B. T.; Lee, Y. I. CuO-Decorated ZnO hierarchical nanostructures as efficient and established sensing materials for H_2S gas sensors. *Sci. Rep.* **2016**, *6*, 26736.

(13) Mukherjee, A.; Rosenwaks, Y. Recent advances in silicon FET devices for gas and volatile organic compound sensing. *Chemosensors* **2021**, *9*, 260.

(14) Fahad, H. M.; Shiraki, H.; Amani, M.; Zhang, C.; Hebbar, V. S.; Gao, W.; Ota, H.; Hettick, M.; Kiriya, D.; Chen, Y. Z.; et al. Room temperature multiplexed gas sensing using chemical-sensitive 3.5-nm-thin silicon transistors. *Adv. Sci.* **2017**, *3*, No. e1602557.

(15) Yuan, Z.; Bariya, M.; Fahad, H. M.; Wu, J.; Han, R.; Gupta, N.; Javey, A. trace-level, multi-gas detection for food quality assessment based on decorated silicon transistor arrays. *Adv. Mater.* **2020**, *32*, No. e1908385.

(16) Hong, S.; Wu, M.; Hong, Y.; Jeong, Y.; Jung, G.; Shin, W.; Park, J.; Kim, D.; Jang, D.; Lee, J. H. FET-type gas sensors: A review. *Sens. Actuators, B* **2021**, *2021*, No. 129240.

(17) Li, J.; Rogers, J. A. Interface engineering of Si hybrid nanostructures for chemical and biological sensing. *Adv. Mater. Technol.* **2020**, *5*, 202000380.

(18) Bondavalli, P.; Legagneux, P.; Pribat, D. Carbon nanotubes based transistors as gas sensors: State of the art and critical review. *Sens. Actuators, B* **2009**, *140*, 304−318.

(19) Zhan, B.; Li, C.; Yang, J.; Jenkins, G.; Huang, W.; Dong, X. Graphene field-effect transistor and its application for electronic sensing. *Small* **2014**, *10*, 4042−4065.

(20) Cao, J.; Chen, Q.; Wang, X.; Zhang, Q.; Yu, H. D.; Huang, X.; Huang, W. Recent development of gas sensing platforms based on 2D atomic crystals. *Research* **2021**, *2021*, 9863038.

(21) Hills, G.; Lau, C.; Wright, A.; Fuller, S.; Bishop, M. D.; Srimani, T.; Kanhaiya, P.; Ho, R.; Amer, A.; Stein, Y.; et al. Modern microprocessor built from complementary carbon nanotube transistors. *Nature* **2019**, *572*, 595−602.

(22) Dürkop, T.; Getty, S. A.; Cobas, E.; Fuhrer, M. S. Extraordinary mobility in semiconducting carbon nanotubes. *Nano Lett.* **2003**, *4*, 35−39.

(23) Lin, Y.; Liang, S.; Xu, L.; Liu, L.; Hu, Q.; Fan, C.; Liu, Y.; Han, J.; Zhang, Z.; Peng, L. M. Enhancement-mode field-effect transistors and high-speed integrated circuits based on aligned carbon nanotube films. *Adv. Funct. Mater.* **2021**, *32*, 2104539.

(24) Zhang, Z.; Liang, X.; Wang, S.; Yao, K.; Hu, Y.; Zhu, Y.; Chen, Q.; Zhou, W.; Li, Y.; Yao, Y.; et al. Doping-free fabrication of carbon nanotube based ballistic CMOS devices and circuits. *Nano Lett.* **2007**, *7*, 3603−3607.

(25) Xiao, M.; Liang, S.; Han, J.; Zhong, D.; Liu, J.; Zhang, Z.; Peng, L. Batch fabrication of ultrasensitive carbon nanotube hydrogen sensors with sub-ppm detection limit. *ACS Sens.* **2018**, *3*, 749−756.

(26) Liu, F.; Xiao, M.; Ning, Y.; Zhou, S.; He, J.; Lin, Y.; Zhang, Z. Toward practical gas sensing with rapid recovery semiconducting carbon nanotube film sensors. *Sci. China Inf. Sci.* **2022**, *65*, No. 162402.

(27) Zhao, Y.; Song, J.; Ryu, G. H.; Ko, K. Y.; Woo, W. J.; Kim, Y.; Kim, D.; Lim, J. H.; Lee, S.; Lee, Z.; et al. Low-temperature synthesis of 2D MoS_2 on a plastic substrate for a flexible gas sensor. *Nanoscale* **2018**, *10*, 9338−9345.

(28) Dresselhaus, M. S.; Dresselhaus, G.; Jorio, A. Raman spectroscopy of carbon nanotubes in 1997 and 2007. *J. Phys. Chem. C* **2007**, *111*, 17887−17893.

(29) Strano, M. S.; Dyke, C. A.; Usrey, M. L.; Barone, P. W.; Allen, M. J.; Shan, H.; Kittrell, C.; Hauge, R. H.; Tour, J. M.; Smalley, R. E. Electronic structure control of single-walled carbon nanotube functionalization. *Science* **2003**, *301*, 1519−1522.

(30) Maultzsch, J.; Telg, H.; Reich, S.; Thomsen, C. Radial breathing mode of single-walled carbon nanotubes: Optical transition energies and chiral-index assignment. *Phys. Rev. B* **2005**, *72*, No. 205438.

(31) Wu, X. Y.; Zhu, L. Y.; Sun, J.; Zhu, K. Y.; Miao, X. Y.; Liu, M. Y.; Zhao, X. F.; Lu, H. L. Pt nanoparticle-modified SnO_2-ZnO core-shell nanosheets on microelectromechanical systems for enhanced H_2S detection. *Acs Appl. Nano Mater.* **2022**, *5*, 6627−6636.

(32) Nagajyothi, P. C.; Pandurangan, M.; Veerappan, M.; Kim, D. H.; Sreekanth, T. V. M.; Shim, J. Green synthesis, characterization and anticancer activity of yttrium oxide nanoparticles. *Mater. Lett.* **2018**, *216*, 58−62.

(33) Dong, H.; Gong, C.; Addou, R.; McDonnell, S.; Azcatl, A.; Qin, X.; Wang, W.; Wang, W.; Hinkle, C. L.; Wallace, R. M. Schottky barrier height of Pd/MoS_2 contact by large area photoemission spectroscopy. *ACS Appl. Mater. Interfaces* **2017**, *9*, 38977−38983.

(34) Suzuki, S.; Bower, C.; Watanabe, Y.; Zhou, O. Work functions and valence band states of pristine and Cs-intercalated single-walled carbon nanotube bundles. *Appl. Phys. Lett.* **2000**, *76*, 4007−4009.

(35) Javey, A.; Guo, J.; Wang, Q.; Lundstrom, M.; Dai, H. Ballistic carbon nanotube field-effect transistors. *Nature* **2003**, *424*, 654−657.

(36) Kim, W.; Javey, A.; Tu, R.; Cao, J.; Wang, Q.; Dai, H. Electrical contacts to carbon nanotubes down to 1 nm in diameter. *Appl. Phys. Lett.* **2005**, *87*, No. 173101.

(37) Senapati, M.; Sahu, P. P. Meat quality assessment using Au patch electrode $AgSnO_2/SiO_2/Si$ MIS Capacitive gas sensor at room temperature. *Food Chem.* **2020**, *324*, No. 126893.

(38) Shin, H.; Kim, D.; Jung, W.; Jang, J.; Kim, Y.; Lee, Y.; Chang, K.; Lee, J.; Park, J.; Namkoong, K.; Kim, I.-D. Surface activity-tuned metal oxide chemiresistor: toward direct and quantitative halitosis diagnosis. *ACS Nano* **2021**, *15*, 14207−14217.

(39) Yin, X.; Dong, L.; Wu, H.; Ma, W.; Zhang, L.; Yin, W.; Xiao, L.; Jia, S.; Tittel, F. Ppb-level H_2S detection for SF_6 decomposition based on a fiber-amplified telecommunication diode laser and a background-gas-induced high-Q photoacoustic cell. *Appl. Phys. Lett.* **2017**, *111*, No. 031109.

(40) Farooque, M.; Fahidy, T. Z. The electrochemical oxidation of hydrogen sulfide in the tafel region and under mass transport control. *J. Electrochem. Soc.* **1978**, *9*, 247−253.

(41) Dong, W.; Xu, C.; Zhao, W.; Xin, M.; Xiang, Y.; Zheng, A.; Dou, M.; Ke, S.; Dong, J.; Qiu, L.; Xu, G. Poisoning effects of H_2S, CS_2, and COS on hydrogen oxidation reaction over Pt/C catalysts. *ACS Appl. Energy Mater.* **2022**, *5*, 12640−12650.

(42) Shivaraman, M. S. Detection of H_2S with Pd-gate MOS field-effect transistors. *J. Appl. Phys.* **1976**, *47*, 3592−3593.

(43) Salomonsson, A.; Eriksson, M.; Dannetun, H. Hydrogen interaction with platinum and palladium metal-insulator-semiconductor devices. *J. Appl. Phys.* **2005**, *98*, No. 014505.

(44) Lundström, K. I.; Shivaraman, M. S.; Svensson, C. M. A hydrogen-sensitive Pd-gate MOS transistor. *J. Appl. Phys.* **1975**, *46*, 3876−3881.

(45) Zhou, S.; Xiao, M.; Liu, F.; He, J.; Lin, Y.; Zhang, Z. Sub-10 parts per billion detection of hydrogen with floating gate transistors built on semiconducting carbon nanotube film. *Carbon* **2021**, *180*, 41−47.

(46) Xu, L.; Gao, N.; Zhang, Z.; Peng, L.-M. Lowering interface state density in carbon nanotube thin film transistors through using stacked Y_2O_3/HfO_2 gate dielectric. *Appl. Phys. Lett.* **2018**, *113*, No. 083105.

(47) Hong, J.; Lee, S.; Seo, J.; Pyo, S.; Kim, J.; Lee, T. A highly sensitive hydrogen sensor with gas selectivity using a PMMA membrane-coated Pd nanoparticle/single-layer graphene hybrid. *ACS Appl. Mater. Interfaces* **2015**, *7*, 3554−3561.